

The speed of the Bacterial Flagellar Motor near zero load depends on the number of stator units

Ashley L Nord^{a,b,1}, Yoshiyuki Sowa^{a,c,1}, Bradley C Steel^a, Chien-Jung Lo^{a,d}, and Richard M Berry^{a,2}

^aDepartment of Physics, University of Oxford, Clarendon Laboratory, Parks Road, Oxford, OX1 3PU UK; ^bSingle Molecule Biophysics Dept., Centre de Biochimie Structurale, CNRS UMR 5048 UM INSERM U 1054, 29 Rue de Navacelles, 34090 Montpellier, France; ^cDepartment of Frontier Bioscience, Hosei University, Tokyo, 184-8584, Japan; ^dDepartment of Physics and Graduate Institute of Biophysics, National Central University, Jhongli, Taiwan 32001, R.O.C.

This manuscript was compiled on September 12, 2017

The bacterial flagellar motor (BFM) rotates hundreds of times per second to propel bacteria, driven by an electrochemical ion gradient. The motor consists of a rotor 50 nm in diameter surrounded by up to 11 ion-conducting stator units which exchange between motors and a membrane-bound pool. Measurements of the torque-speed relationship guide the development of models of the motor mechanism. In contrast to previous reports that speed near zero torque is independent of the number of stator units, we observe multiple speeds that we attribute to different numbers of units near zero torque in both Na⁺ and H⁺-driven motors. We measure the full torque-speed relationship of one and two H⁺ units in *Escherichia coli* by selecting the number of H⁺ units and controlling the number of Na⁺ units in hybrid motors. These experiments confirm that speed near zero torque in H⁺-driven motors increases with the stator number. We also measured 75 torque-speed curves for Na⁺-driven chimeric motors at different ion-motive force and stator number. Torque and speed were proportional to ion-motive force and number of stator units at all loads, allowing all 77 measured torque-speed curves to be collapsed onto a single curve by simple re-scaling.

Bacterial Flagellar Motor | molecular motor | hybrid-fuel motor | *Escherichia coli* | motility

At high load in *E. coli*, each stator unit is exchanged every ~30 s (1), and stator units leave the motor when the ion-motive force is removed (2–4). Natural (5, 6) and artificial (7) hybrid-fuel motors exist, in which H⁺- and Na⁺ stators are co-expressed. BFMs combining the rotor of *E. coli* with chimeric Na⁺-driven stator units containing PomA from *Vibrio alginolyticus* and a fusion of MotB from *E. coli* and PomB from *V. alginolyticus* (8) have been used for many mechanistic studies. Measured torque in H⁺ and Na⁺ motors with various numbers of stator units (9–13) is nearly constant up to a so-called “knee” speed, falling more steeply to zero at higher speeds. Both the knee- and zero-torque speeds increase with temperature and, at high sodium concentrations (85 mM), are higher for Na⁺- than for H⁺- motors.

Extrapolations of torque-speed curves predicted that the speed of the H⁺-driven motor at zero load is independent of unit number (9). The observation of only one speed of gold nanoparticles attached to the hook of H⁺-driven motors lacking a flagellar filament, at expression levels of stator proteins that give many units at high load, appeared to support this prediction – under the assumption that these motors also contained many units (14). However, the recent discovery that motors contain fewer units at lower load (15, 16) invalidates this assumption. Furthermore, Na⁺-driven motors show multiple speeds at low load (13). These results reopen the question of how the zero-load speed depends upon unit number and indicate that previous torque-speed measurements likely conflated properties of stator units with load-dependent stator

recruitment.

Here, we demonstrate that speed at low load increases approximately linearly with the number both of Na⁺- and H⁺-driven stator units. We measure 75 torque-speed relationships for chimeric motors driven by 1–3 Na⁺ units and a wide range of electrical and chemical potentials. We also measure, in individual hybrid-fuel motors, torque-speed curves for 1 and 2 H⁺ units; by using Na⁺ stator units operating in their constant-torque regime to push H⁺ units in the same motor up to and beyond their zero-torque speed. We rescale torque and speed, dividing each by ion-motive force (IMF) and stator number and further dividing speed by an empirical function of ion concentration, to obtain a single torque-speed curve that describes flagellar motors in *E. coli* at all 77 different measured combinations of driving ion, chemical and electrical potential, and number of stator units.

Results

Na⁺ motor at low load. Gold nanoparticles 100 nm in diameter were attached to hooks of Na⁺-driven chimeric motors lacking flagellar filaments. Motor speeds were monitored via backscattering darkfield microscopy (17). These recordings were combined with previous data acquired in the same manner (13). Fig. 1A shows a typical trace where 85 mM Na⁺ was transiently removed ($t \sim 20 - 75$ s). The speed of the motor quickly dropped to zero with Na⁺ removal and increased in step-wise increments after Na⁺ was reintroduced, a typical signature of the removal and addition of torque-generating stator units (7, 18). Fig. 1B–D show examples of sponta-

Significance Statement

The bacterial flagellar motor is a rotary molecular motor responsible for swimming, swarming, and chemotaxis in many species of bacteria. It generates torque by interactions between a rotor 50 nm in diameter and multiple stator units. We overturn the prevailing understanding of how stator units interact with each other by showing that motor speed is dependent upon the number of stator units even at high speed, near zero torque. We describe a new method to measure torque and speed that uses synthetic hybrid stators driven by different ion types, and show that with simple re-scaling a single torque-speed curve describes the motor over widely varying values of the membrane voltage, driving ion type and ionic chemical potential gradient.

YS, ALN, BCS and CL collected the experimental data; ALN, RMB, and BCS wrote the data analysis software; ALN and YS analyzed the data; ALN, YS and RMB wrote the manuscript.

The authors declare that they have no competing financial interests.

¹ALN and YS contributed equally to this work.

²To whom correspondence should be addressed. E-mail: richard.berry@physics.ox.ac.uk

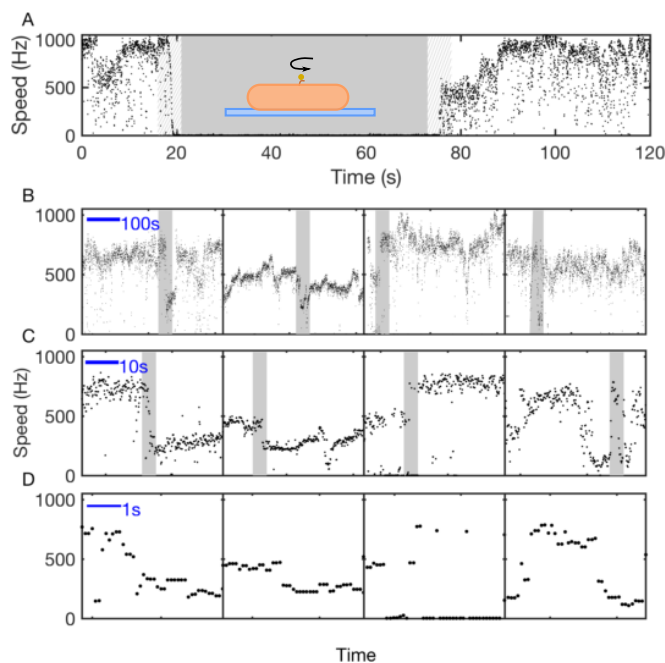


Fig. 1. Discrete speed levels of the Na^+ -driven motor at low load. (A) Speed vs. time for a 100 nm gold bead attached to the hook of single Na^+ -driven chimeric flagellar motor. Na^+ was removed between ~ 20 s and 75 s (shading). The inset shows a schematic of the experimental assay. (B–D) Typical speed time traces at pH 7 in 85 mM $[\text{Na}^+]$. Transitions between distinct speed levels are seen on timescales ranging from seconds to minutes. Shaded portions in (B) and (C) are shown in (C) and (D), respectively.

neous step-wise speed changes in 85 mM Na^+ , similar to those previously observed with larger loads (13, 19), presumably corresponding to the loss or gain of a stator unit. Similar examples for other $[\text{Na}^+]$ are shown in Fig. ???. Each motor often showed zero or low speed, especially at low $[\text{Na}^+]$. Fig. 2A shows histograms of motor speed driving 100 nm gold nanoparticles for five different $[\text{Na}^+]$, ranging from 1 mM to 85 mM. As observed previously (13), the speed histograms show clear multiple peaks, indicating multiple speed levels at very low load. Speed histograms were fit as a sum of Gaussians, with the peak of each Gaussian defining a speed level corresponding to a particular configuration of the motor. These configurations have always previously been assumed to correspond to different numbers of stator units (9, 14, 19–21), which is our starting assumption.

Torque-Speed curves of the Na^+ motor. Fig. 2B shows torque-speed curves of the Na^+ -driven motor driven by one, two, or three stator units at pH 7 and the same values of $[\text{Na}^+]$ as Fig. 2A. Speeds correspond to Gaussian peaks in speed histograms for motors driving gold beads (coloured circles and Fig. 2A) and similarly for motors driving polystyrene beads of diameter 0.2–1.0 μm attached to truncated filaments of the Na^+ -driven motor (13) (black circles). Torque was calculated as speed times the rotational frictional drag coefficient of each size of bead. The dataset of speeds of polystyrene beads was the same as that used by Lo et al (13). Black dashed lines link the lowest speed levels observed with polystyrene and 100 nm gold beads at each $[\text{Na}^+]$. The lowest speed levels observed with gold beads in 10, 5 and 1 mM Na^+ were faster than expected for single stator units, given the concave-down shape

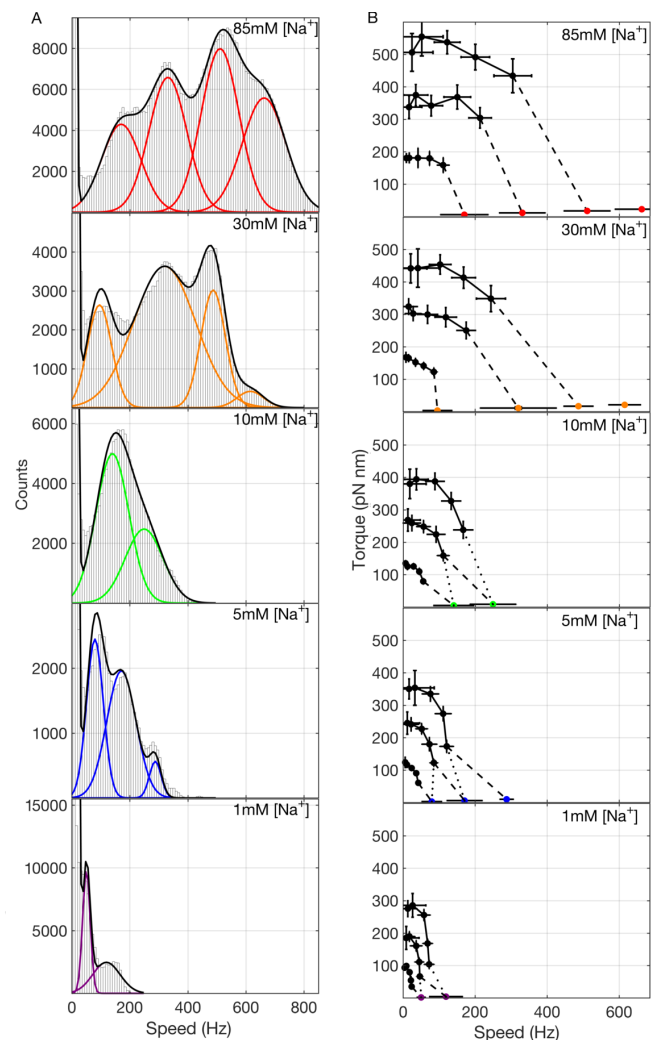


Fig. 2. Torque and speed of the Na^+ -driven motor at pH 7 for varying $[\text{Na}^+]$. (A) Histograms of speeds of 100 nm gold beads attached to Na^+ -driven motors, from records such as those illustrated in Fig. 1B–D. Distinct peaks in the histograms are fit (black line) as a sum of Gaussians (coloured lines). Speeds from 56, 44, 28, 40, 51 different motors were combined for 85, 30, 10, 5 and 1 mM $[\text{Na}^+]$ respectively. (B) Torque-speed curves of Na^+ -driven motors with 1–3 stator units at pH 7.0 and varying $[\text{Na}^+]$. Colored symbols show speeds from the Gaussian fits in (A). Black symbols show previously published speeds of polystyrene beads on flagellar filaments (13). Black solid lines connect measurements of motors with the same presumed number of stators. Black dashed lines indicate an inference of the correspondence between numbers of stators in the polystyrene and gold bead data, based upon the assumption that the lowest speed corresponds to a single stator unit. Black dotted lines indicate an alternative inference, based upon the assumption that some speed levels have not been resolved in the gold bead data at 1, 5, and 10 mM $[\text{Na}^+]$. Data points indicate means and error bars indicate SDs.

of the torque-speed curves for higher $[\text{Na}^+]$ and for polystyrene beads. Given the variance in speed for each speed level, we would not expect to resolve any level below ~ 100 Hz and the most likely explanation is that single-unit speed levels are not resolved by Gaussian fitting at low $[\text{Na}^+]$. Dotted lines in Fig. 2B link gold to polystyrene data under the assumption that the lowest resolved speed levels with gold represent motors with 2 stator units at 10, 5 and 1 mM $[\text{Na}^+]$.

Under this assumption, the torque-speed curves for motors with 1–3 stator units all share the characteristic concave-down shape previously reported for motors with one (22) and many

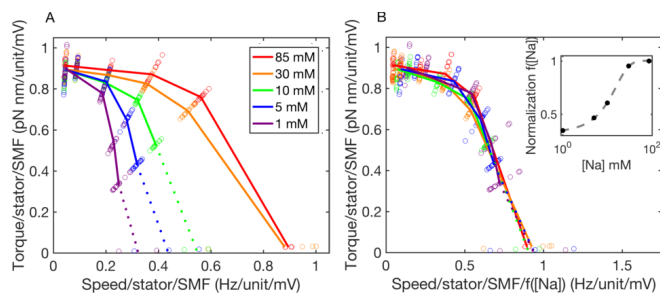


Fig. 3. Normalized torque-speed curves of the Na^+ -driven motor. (A) 75 individual torque-speed curves similar to those of Fig. 2, but including data obtained at pH 5, 5.5, 6, 6.5 and 7, and with both torque and speed normalized by the number of stator units and the SMF, the latter estimated from pH and $[\text{Na}^+]$ as described (25). Coloured lines (corresponding to Fig. 2) show averages for each $[\text{Na}^+]$ over stator number and pH. This plot combines data from this study and two previous studies (13, 25), showing average measurements from 396 combinations of bead size, $[\text{Na}^+]$, pH, and stator unit number. (B) The same as (A), but with speeds further divided by an empirical normalizing function $f([\text{Na}^+])$ (inset, fit by a logistic function, dashed) that collapses all 75 torque-speed curves onto a single curve. Dotted lines assign gold bead stator number under the assumption that some speed levels are not resolved for 1, 5, and 10 mM $[\text{Na}^+]$.

(9–12, 22–24) units. The zero-torque speed and the stall torque are both approximately proportional to unit number (see Fig. ??). Torque-speed curves obtained similarly but with polystyrene beads only, at a range of pH values corresponding to a range of values of the membrane voltage (13, 25), all showed the same qualitative features (see Fig. ??). Fig. 3A combines all 75 chimeric motor torque-speed curves, comprising a filled $5 \times 5 \times 3$ matrix corresponding to 5 different values of membrane voltage, 5 different $[\text{Na}^+]$, and 1–3 stator units, normalized by dividing each torque and each speed by both the number of stator units and the sodium-motive force (25). The same colours as Fig. 2 are used to mark each value of $[\text{Na}^+]$, and lines show averages over membrane voltage and number of stator units. This demonstrates that both torque and speed at each sodium concentration are proportional to both sodium motive force (SMF) and the number of units, under all conditions and all viscous loads measured. Fig. 3B collapses all 75 curves onto a single torque-speed curve, after further normalizing speed by dividing by an empirical function $f([\text{Na}^+])$ (inset), with values at each measured $[\text{Na}^+]$ chosen by hand to maximize the overlap of the resulting curves. While it is evident that $[\text{Na}]$ has an effect over and above its effect on the SMF, the mechanistic explanation for $f([\text{Na}^+])$ remains to be discovered. Fig. ??D,E show the alternative assignment of stator numbers to gold bead data.

H^+ motor at low load. The speed of H^+ -driven motors in motility buffer near zero load was investigated in a manner similar to Na^+ -driven motor experiments above. Fig. 4A–C show examples of spontaneous step-wise speed changes similar to those of the Na^+ motor in Fig. 1, and Fig. 4D the histogram of all speeds recorded from 59 different motors driving 100 nm gold nanoparticles. As the distribution shows at least two evident peaks, we applied a two-Gaussian fit (blue line). The highest of these speed levels is similar to the single speeds previously reported in similar experiments (14, 26), while lower speeds have not previously been reported.

Torque-Speed curves of H^+ -driven stator units. We took advantage of the hybrid-fuel motor, in which the torques gener-

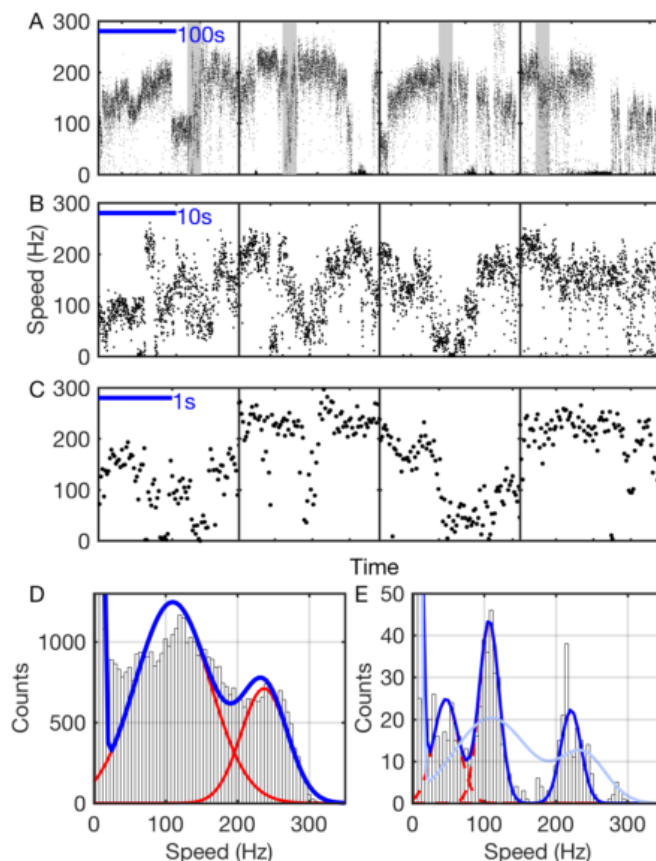


Fig. 4. Discrete speed levels of the H^+ -driven motor at low load. (A–C) Typical speed time traces for 100 nm gold beads attached to the hook of single H^+ -driven (wild-type) flagellar motors. As with Na^+ motors in Fig. 1B–D, transitions between distinct speed levels are seen on timescales ranging from seconds to minutes. Data shown in (A) were acquired at 20 kHz, and shaded portions in (A) are shown in (B). Separate traces, shown in (C), were acquired at 109.5 kHz. (D) Histogram of speeds of 100 nm gold beads attached to H^+ driven motors, from records such as those illustrated in (A–C) (8 cells (1394 s) acquired at 20 kHz on the QPD and 51 cells (53 s) acquired at 109.5 kHz on a CMOS camera). Distinct speed levels are seen as peaks in the histogram and fit (blue line) as a sum of Gaussians (red lines). (E) Histogram of the subset (96%, 8 cells) of data in (D) that was acquired in continuous blocks longer than 9 s, downsampled and filtered to match the time resolution of previous low load data (14) (see SI). The distribution was fit (blue line) as a sum of Gaussians (red lines). The scaled distribution of (D) is overlaid (light blue).

ated by Na^+ and H^+ stator units upon a common rotor were found simply to sum (7), to measure the complete torque-speed curves of single or pairs of H^+ -driven stator units. Fig. 5A shows speed versus time of a 0.5 μm bead attached to the truncated filament of a hybrid-fuel motor at pH 7 in a cell with low level induction of H^+ stator proteins, MotA/MotB, and high level induction of Na^+ stator proteins, PomA/PotB. Initially, the motility medium contained no sodium, guaranteeing that any rotating motors were driven only by H^+ units (4, 18). Under these conditions, motor speeds have previously been determined to be about 30 Hz per H^+ unit (9). We selected motors driven initially by either one (~ 30 Hz) or two (~ 60 Hz) H^+ stator units, and measured speeds while the sodium-free buffer was transiently replaced by 85 mM Na^+ buffer. Fig. 5A,D show speed versus time for examples of one- and two- H^+ -unit motors respectively, with shading indicating the presence of sodium. Motor speed increased in step-wise increments upon addition of sodium, and decreased

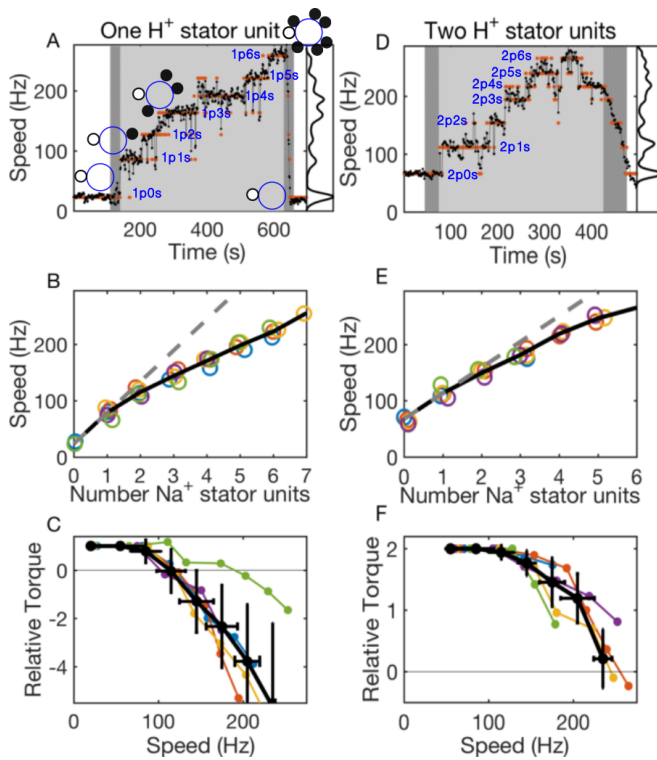


Fig. 5. Torque-speed curves for one and two H⁺ stator units measured in hybrid-fuel motors. (A,D) Typical speed vs. time traces of motors containing (A) one and (D) two H⁺ stator units, with a speed histogram on the right. Orange dots show the speed level of each data point assigned by k-means clustering. Light and dark shading indicate 85 mM [Na⁺] and transitions between 0 to 85 mM [Na⁺], respectively. Na⁺ stator units are recruited in 85 mM [Na⁺]; interpretations of the number and type of units engaged in the motor are shown, where *mps* indicates *m* H⁺ units and *n* Na⁺ units. (B,E) Speed vs. the number of Na⁺ units, for all motors that showed the same speed before and after addition of 85 mM [Na⁺] (5 motors each). Each motor in each plot is shown in a different colour; the motors from (A,D) are shown in orange. The black solid line connects the mean speed of all the motors for each number, and the black dashed line is a linear fit to the points of the first three (B) or two (E) units (those for which motor speed is less than 115 Hz, the approximate position of the 'knee' of the torque-speed curve). (C,F) Calculated torque-speed curves for one and two H⁺ stator units. Colours match those in (B,E). The black line shows average torque-speed curves (mean \pm SD), with each point an average over speed bins of width 40 Hz.

rapidly following the removal of sodium several minutes later, as seen in previous resurrection experiments with larger beads on the hybrid-fuel motor (7). In 10 out of 43 cases, the motor returned to the speed measured before the introduction of sodium buffer. We calculated torque-speed curves for these cases under the assumption that the same number of H⁺ stator units remained in these motors throughout.

Discrete speed levels were determined using k-means clustering, and orange dots in Fig. 5A,D show the speed level assigned to each data point. The corresponding interpretations of the number and type of stator units engaged (1 additional Na⁺ unit for each speed level) are also shown. It has previously been demonstrated that the resurrection of Na⁺ units within a motor causes equal speed increments up to a speed of 400 Hz (12), indicating that there is no change in the torque generated per Na⁺ unit in this speed range. Fig. 5B,E, by contrast, show reducing speed increments with the addition of Na⁺ units at speeds above \sim 115 Hz, consistent with the expected decrease in torque generated by the H⁺ unit(s) at

higher speeds. Assuming the total torque is the sum of independent contributions from *m* H⁺ and *n* Na⁺ stator units (denoted *mp*, *ns*), and that each Na⁺ unit generates a constant torque at all speeds observed in these experiments, we may write the balance between motor torque and viscous drag as

$$\gamma\omega = \tau_{ns} + \tau_{mp} = n\tau_{1s} + \tau_{mp} \quad [1]$$

where γ is the combined rotational drag coefficient of the filament stub and bead, ω is the measured speed, and τ_{xy} is the torque generated by *x* stator units of type *y*. Assuming that at low speeds each H⁺ stator unit generates a constant torque (19), we divide equation (1) by the torque generated by a single H⁺ stator at low speeds,

$$\tau_{1p}^0 = \frac{\gamma\omega_0}{m} \quad [2]$$

where ω_0 is the measured speed in the absence of Na⁺ stator units. This defines a relative H⁺ stator unit torque

$$\tau_{rel} = \frac{\tau_{mp}}{\tau_{1p}^0} = m \left(\frac{\omega - n\omega_{1s}}{\omega_0} \right) \quad [3]$$

where $\omega_{1s} = \tau_{1s}/\gamma$ is the difference between the lowest two speed levels determined by k-means clustering. The average value of ω_{1s} was 57 ± 10 Hz and 46 ± 5 Hz in one and two H⁺ stator unit motors respectively, in agreement with previous measurements (13). Fig. 5C,F show τ_{rel} versus ω for individual motors (colours), and the corresponding average torque-speed curves (black). By exploiting the higher characteristic speed of Na⁺ stator units at high sodium concentration, this method allows determination of torque-speed curves of a single or a pair of H⁺ unit(s) up to and beyond zero load without the need to apply external torque. The zero-torque speeds for one and two H⁺ stator units are \sim 120 Hz and \sim 240 Hz, respectively, confirming our independent observation of multiple speed levels near zero load with gold nanospheres (Fig. 4).

Discussion

In this study we have observed that both H⁺ and Na⁺-driven flagellar motors in *E. coli* show multiple speed levels near zero-load. Thus, contrary to previous assumptions, the zero-torque speed of the BFM is not independent of stator unit number, requiring a reassessment of mechanistic models of the BFM. We have developed a novel method allowing the first measurement of the entire torque-speed curves of 1 and 2 H⁺-driven stator units in individual motors, and obtained 77 different torque-speed curves for H⁺- and Na⁺-driven motors with a range of ion motive forces and numbers of stator units. Both torque and speed are approximately proportional to both ion motive force and number of stator units for all viscous loads measured, and with simple re-scaling all 77 torque-speed curves collapse onto a single curve (see Fig. ??C) with the previously reported concave-down shape (9–13) characteristic of counterclockwise (CCW) rotation in *E. coli*.

This is in contrast to the linear torque-speed curve reported for clockwise (CW) rotation (27). We speculate that the CCW torque-speed relationship may indicate selection pressure for high power output, as it combines high torque and high speed at viscous drag coefficients similar to those experienced in the bundle of a swimming *E. coli* cell. By contrast, the linear relationship seen in CW rotation is easier to achieve

in mechanistic models and may represent a lack of selection pressure, given that CW rotation is not typically used to propel swimming. If so, we predict that species in which both rotation directions are selected for swimming will show concave-down torque-speed curves in both directions.

If torque and speed are proportional to the number of units beyond 3 in other species, those with additional stator structures that are thought to maintain high numbers of stator units (28) are predicted to rotate above 1000 Hz at low load. We note that the speed per unit per mV of IMF of the H^+ motor at pH 7 is roughly the same as that of the chimeric motor at saturating $[Na^+]$, despite a \sim million-fold difference in ion concentration. This anomalously high rate of proton arrival presumably indicates some or all of: enhanced proton mobility near the lipid membrane (29), diffusion by the Grotthuss mechanism (30), and delivery of protons to the motor by buffer species. If ion arrival is the rate-limiting step at low load, equal arrival rates for H^+ and Na^+ may simply be a co-incidence. If ion transit or conformational changes in the motor are limiting, this may point to common mechanisms for these processes in both types of stator.

Our novel method of controlling hybrid motor speed with Na^+ stator units avoids the problems of angular variation and mechanical or photo-damage associated with previous measurements of the torque-speed relationship of a single motor, using electrorotation (22, 24) or laser trapping of a bead duplex (31). Furthermore, because Na^+ -stator torque is applied directly to the rotor, potential artifacts due to flexible hook interactions (32) are also avoided. This method measured zero-load speeds of about 120 and 240 Hz for one and two stator units respectively, in good agreement with our data from gold beads, supporting the conclusion that the zero-load speed depends upon the number of stator units in the H^+ motor as well as in the Na^+ motor.

This is the most striking discrepancy between our results and previous literature. Previously, it was reported that H^+ -driven motors jump suddenly between not rotating and rotating at a maximum speed between 250 and 300 Hz, with no intermediate speed levels (14). In our study, while some motors were observed to rotate continuously at a single speed over many seconds, similar to those reported previously (14), most showed extensive speed changes as shown in Fig. 4. The 4.6-fold difference in viscous drag coefficient between our 100 nm beads and the 60 nm beads used previously (14) (an upper limit, assuming rotation about a diameter) is unlikely to explain this discrepancy, as in both cases the loads are very low. We tested several alternative hypotheses. Our data were acquired at 20 kHz or 109.5 kHz and speeds calculated over 0.02 s intervals, those of the previous study (14) at 3 kHz and speeds calculated over 1 s intervals then median filtered, rank 4, to yield a time resolution of \sim 9 s, 450 times slower than ours. Our high time resolution may explain the relatively noisy speed traces for both H^+ and Na^+ motors. Given the spatial and temporal resolution of our measurements, this noise is representative of the motor, rather than an artifact of measurement. Analysis of speed histograms, however, extracts discrete speed levels without loss of time resolution. Downsampling and filtering a subset of our data traces (with sufficiently long duration) to match the procedures of the previous study (14), returned peaks at 107 ± 14 Hz, and 215 ± 47 Hz, similar to our original analysis, plus an additional peak at 47 ± 18 Hz

that might represent an average of switching between zero and the lowest level that is resolved at our original time-resolution but not after downsampling (Fig. 4E). We excluded the alternative possibility that lower speed levels in our experiments are a consequence of photodamage, under the assumption that our laser intensity (100 W/cm^{-2}) was greater than that used previously (14), by observing a lack of intensity dependence of rotation of gold beads attached to H^+ motors over more than a 4-fold range of laser intensities (see Fig. ??).

The discrepancy between our results and previous results (14) remains unexplained. Given previous literature and our new Na^+ data, the simplest interpretation of our observation of the same two distinct speeds near zero torque in the H^+ motor using two totally different methods (steady state recording with gold beads and measurement of the torque-speed curve of the proton stator in the hybrid motor) is that the speed levels correspond to one and two stator units. Testing this interpretation with simultaneous determination of stator number by fluorescence microscopy is beyond our current experimental capabilities, and very low yields of rotating motors at low loads, combined with short recording times in our high-speed setup, prevent us from identifying single-unit motors using initial speed levels in ‘resurrection’ experiments (19). We attempted to observe speed levels corresponding to 3 or more H^+ units by overexpression of stator proteins. Induction with $1 \mu\text{M}$ arabinose yielded zero spinning motors, while $10 \mu\text{M}$, $20 \mu\text{M}$, and 1 mM arabinose were indistinguishable in both yield and motor speed. We hypothesize either that the concentration of stator proteins is not limiting in our experiments, or that our expression system is saturated at $10 \mu\text{M}$ arabinose; and that either the affinity at low load or the expression level of sodium stator units is greater than those of the proton stator, allowing for observation of higher stator numbers. Without these tests the possibility remains that Na^+ and H^+ stators are different at low load, and alternative interpretations of discrete speed levels in the H^+ motor need to be considered. If a fully functional unit rotates at 240-300 Hz (14), lower speed levels might represent partially functional units. Speculations as to the possible nature of these include units attached to the peptidoglycan at sub-optimal orientations or distances from the rotor, and half-functional units with one channel either blocked, mis-folded or otherwise mis-assembled.

The torque-speed relationships of motors driven by Na^+ and H^+ stators are very similar, indicating that the motor mechanism is shared by both ion types. In order to fit the previously held experimental constraint of zero-load speeds independent of stator unit number, mechanistic motor models have invoked three conditions: 1) compliant springs linking stator units to the cell wall, storing energy and allowing stator units to step independently (33, 34); 2) high duty ratio, such that the stator units remain attached to the rotor most of the time (9); and 3) load-independence of rate constants for forwards transitions of the motor which are rate-limiting at low load (9). Our results lift this constraint. Lifting condition 3) in a model where rotation and ion transit are tightly-coupled, and thus the duty ratio is 1, causes the zero-load speed to increase with stator number (9), and with suitable parameters might be able to reproduce the observed approximate linear dependence for 1-3 stator units (Fig. ??). Loose coupling and low duty ratio also reproduce approximately linear dependence on stator number (9, 35). Loose coupling is one possible explanation for

the discrepancy between observations of 26 steps per revolution with one stator unit (18) and an estimate that at least 37 ions pass through the Na⁺-driven motor per stator unit per revolution (13). Recent models have proposed loose coupling either where torque-generating conformational changes in a stator unit can be driven by either one or two ions (36), or where coupling between ions and stator unit conformation change is tight, but the duty ratio is less than one at low load (35). Our data leave open the question of stator springs. Finally, we note the possibility that the observed 26 steps per revolution are a signature of a passive periodic structure in the motor rather than of the mechanochemical cycle (33).

Materials and Methods

Refer to SI for further details regarding materials and methods.

Bacteria and culture. *E. coli* strains (7, 8, 18, 21, 37–39) were grown and stator proteins were induced as described previously (7).

Speed Measurements. Cells were immobilised on poly-L-lysine coated glass coverslips in custom-made flow chambers. Particles were attached to the hook or truncated flagella as described previously (7, 14, 38). Beads were tracked using either back-focal-plane interferometry (7, 40) or back-scattering darkfield microscopy (17) and a quadrant photodiode (QPD) or CMOS camera (Photron). All experiments were performed at 23°C in motility buffer (7).

Motor speed analysis. Speeds were analysed using custom Labview and MATLAB programs from power spectra of the (x,y) position of the bead, similar to performed previously, (9) (see SI). A multiple Gaussian fit was applied to speed histograms. For hybrid motor experiments, speeds were clustered using the k-means (41) and G-means (42) algorithms.

Torque calculation. Motor torque was calculated as $\tau = (f_b + f_f)\omega$, where ω is the angular velocity, and f_b and f_f are the rotational frictional drag coefficients of the attached bead and filament stub (where present), respectively (12).

1 and 2 H⁺ stator torque-speed curves. In Fig. 5A,C, the number of H⁺ stator units engaged prior to Na⁺ buffer addition and after Na⁺ buffer removal was assigned according to motor speed. The number of Na⁺ stators engaged was assigned by adding one for each speed level. In Fig. 5C,F, each point in the average curve (black) shows the mean and SD of all of the points from the individual curves (shown in colours) falling within a bin width of 40Hz.

ACKNOWLEDGMENTS. ALN was supported by the Rhodes Trust and YS was supported by KAKENHI and JSPS-Abroad. This work was also supported by BBSRC grants BB/H01991X/1 and BB/E00458X/1. We thank Howard C. Berg for the gift of anti-FlgE antibody. CBS is a member of the France-Biologimaging (FBI) and the French Infrastructure for Integrated Structural Biology (FRISBI), two national infrastructures supported by the French National Research Agency (ANR-10-INBS-04-01 and ANR-10-INBS-05).

1. Leake MC, et al. (2006) Stoichiometry and turnover in single, functioning membrane protein complexes. *Nature* 443:355–358.
2. Tipping MJ, Steel BC, Delalez NJ, Berry RM, Armitage JP (2013) Quantification of flagellar motor stator dynamics through in vivo proton-motive force control. *Mol. Microbiol.* 87(2):338–347.
3. Sowa Y, Berry RM (2008) Bacterial flagellar motor. *Q. Rev. Biophys.* 41(2):103–132.
4. Fukuoka H, Wada T, Kojima S, Ishijima A, Homma M (2009) Sodium-dependent dynamic assembly of membrane complexes in sodium-driven flagellar motors. *Mol. Microbiol.* 71(4):825–835.
5. Paulick A, et al. (2009) Two different stator systems drive a single polar flagellum in *Shewanella oneidensis* mr-1. *Mol. Microbiol.* 71(4):836–850.
6. Paulick A, et al. (2015) Dual stator dynamics in the *Shewanella oneidensis* mr-1 flagellar motor. *Molecular microbiology* 96(5):993–1001.
7. Sowa Y, Homma M, Ishijima A, Berry RM (2014) Hybrid-fuel bacterial flagellar motors in *Escherichia coli*. *Proc. Natl. Acad. Sci. U.S.A.* 111(9):3436–3441.
8. Asai Y, Yakushi T, Kawagishi I, Homma M (2003) Ion-coupling determinants of Na⁺-driven and H⁺-driven flagellar motors. *J. Mol. Biol.* 327(2):453–63.

9. Ryu WS, Berry RM, Berg HC (2000) Torque-generating units of the flagellar motor of *Escherichia coli* have a high duty ratio. *Nature* 403(6768):444–7.
10. Sowa Y, Hotta H, Homma M, Ishijima A (2003) Torque-speed relationship of the Na⁺-driven flagellar motor of *Vibrio alginolyticus*. *J. Mol. Biol.* 327(5):1043–51.
11. Chen X, Berg HC (2000) Torque-speed relationship of the flagellar rotary motor of *Escherichia coli*. *Biophys. J.* 78(2):1036–41.
12. Inoue Y, et al. (2008) Torque-speed relationships of Na⁺-driven chimeric flagellar motors in *Escherichia coli*. *J. Mol. Biol.* 376(5):1251–9.
13. Lo CJ, Sowa Y, Pilizota T, Berry RM (2013) Mechanism and kinetics of a sodium-driven bacterial flagellar motor. *Proc. Natl. Acad. Sci. U.S.A.* 110(21):E2544–51.
14. Yuan J, Berg HC (2008) Resurrection of the flagellar rotary motor near zero load. *Proc. Natl. Acad. Sci. U.S.A.* 105(4):1182–5.
15. Lele PP, Hosu BG, Berg HC (2013) Dynamics of mechanosensing in the bacterial flagellar motor. *Proc. Natl. Acad. Sci. U.S.A.* 110(29):11839–44.
16. Tipping MJ, Delalez NJ, Lim R, Berry RM, Armitage JP (2013) Load-dependent assembly of the bacterial flagellar motor. *mBio* 4(4).
17. Sowa Y, Steel BC, Berry RM (2010) A simple backscattering microscope for fast tracking of biological molecules. *Rev. Sci. Instrum.* 81(11):113704.
18. Sowa Y, et al. (2005) Direct observation of steps in rotation of the bacterial flagellar motor. *Nature* 437(7060):916–9.
19. Reid SW, et al. (2006) The maximum number of torque-generating units in the flagellar motor of *Escherichia coli* is at least 11. *Proc. Natl. Acad. Sci. U.S.A.* 103(21):8066–71.
20. Block SM, Berg HC (1984) Successive incorporation of force-generating units in the bacterial rotary motor. *Nature* 309(5967):470–2.
21. Blair DF, Berg HC (1988) Restoration of torque in defective flagellar motors. *Science* 242(4886):1678–81.
22. Berry RM, Berg HC (1999) Torque generated by the flagellar motor of *Escherichia coli* while driven backward. *Biophys. J.* 76(1 Pt 1):580–7.
23. Nakamura S, et al. (2009) Effect of intracellular pH on the torque-speed relationship of bacterial proton-driven flagellar motor. *J. Mol. Biol.* 386(2):332–338.
24. Berg HC, Turner L (1993) Torque generated by the flagellar motor of *Escherichia coli*. *Biophys. J.* 65(5):2201–16.
25. Lo CJ, Leake MC, Pilizota T, Berry RM (2007) Nonequivalence of membrane voltage and ion-gradient as driving forces for the bacterial flagellar motor at low load. *Biophys. J.* 93(1):294–302.
26. Yuan J, Berg HC (2010) Thermal and solvent-isotope effects on the flagellar rotary motor near zero load. *Biophys. J.* 98(10):2121–2126.
27. Yuan J, Fahrner KA, Turner L, Berg HC (2010) Asymmetry in the clockwise and counterclockwise rotation of the bacterial flagellar motor. *Proc. Natl. Acad. Sci. U.S.A.* 107(29):12846–12849.
28. Beeby M, et al. (2016) Diverse high-torque bacterial flagellar motors assemble wider stator rings using a conserved protein scaffold. *Proc. Natl. Acad. Sci. U.S.A.* 113(13):1917.
29. Yoshinaga MY, Kellermann MY, Valentine DL, Valentine RC (2016) Phospholipids and glycolipids mediate proton containment and circulation along the surface of energy-transducing membranes. *Progress in Lipid Research* 64:1–15.
30. Prats M, Teissie J, Tölgner JF (1986) Lateral proton conduction at lipid-water interfaces and its implications for the chemiosmotic-coupling hypothesis. *Nature* 322(6081).
31. Berry RM, Berg HC (1997) Absence of a barrier to backwards rotation of the bacterial flagellar motor demonstrated with optical tweezers. *Proc. Natl. Acad. Sci. U.S.A.* 94(26):14433–7.
32. Hashimoto M, Mashimo T, Hirano T, Yamaguchi S, Aizawa S (2008) Functional roles of the hook in a rotating tethered cell. *J. Mol. Biol.* 375(2):367–75.
33. Mora T, Yu H, Wingreen NS (2009) Modeling torque versus speed, shot noise, and rotational diffusion of the bacterial flagellar motor. *Phys. Rev. Lett.* 103(24):248102.
34. Bai F, Lo CJ, Berry RM, Xing J (2009) Model studies of the dynamics of bacterial flagellar motors. *Biophys. J.* 96(8):3154–67.
35. Nirody J, Berry R, Oster G (2016) The limiting speed of the bacterial flagellar motor. *Biophys. J.* 111(3):557–564.
36. Boschert R, Adler FR, Blair DF (2015) Loose coupling in the bacterial flagellar motor. *Proc. Natl. Acad. Sci. U.S.A.* 112(15).
37. Nord AL, Pedaci F, Berry RM (2016) Transient pauses of the bacterial flagellar motor at low load. *New Journal of Physics* 18(11).
38. Brown MT, et al. (2012) Flagellar hook flexibility is essential for bundle formation in swimming *Escherichia coli* cells. *J. Bacteriol.* 194(13):3495–3501.
39. Scharf BE, Fahrner KA, Turner L, Berg HC (1998) Control of direction of flagellar rotation in bacterial chemotaxis. *Proc Natl Acad Sci U S A* 95(1):201–6.
40. Rowe AD, Leake MC, Morgan H, Berry RM (2003) Rapid rotation of micron and submicron dielectric particles measured using optical tweezers. *J. Mod. Opt.* 50(10):1539–54.
41. MacQueen J (1967) Some methods for classification and analysis of multivariate observations. *Proc. Fifth Berkeley Symp. on Math. Statist. and Prob.* 1:281–297.
42. Hamerly G, Elkan C (2003) Learning the k in k-means in *Annual conference on neural information processing systems (NIPS)*. No. 17, pp. 281–288.
43. Chen X, Berg HC (2000) Solvent-isotope and pH effects on flagellar rotation in *Escherichia coli*. *Biophys. J.* 78(5):2280–4.
44. Hirano T, Yamaguchi S, Oosawa K, Aizawa S (1994) Roles of fliK and fliH in determination of flagellar hook length in *Salmonella typhimurium*. *J. Bacteriol.* 176(17):5439–49.
45. Happel J, Brenner H (1991) *Low Reynolds Number Hydrodynamics*. (Martinus Nijhoff Publishers, Columbia University).
46. Gabel CV, Berg HC (2003) The speed of the flagellar rotary motor of *Escherichia coli* varies linearly with protonmotive force. *Proc. Natl. Acad. Sci. U.S.A.* 100(15):8748–51.
47. Betzig E, et al. (2006) Imaging intracellular fluorescent proteins at nanometer resolution. *Science* 313(5793):1642.
48. Schwarz G (1978) Estimating the dimension of a model. *Ann. Stat.* 6(2):461–464.
49. Parkinson JS (1978) Complementation analysis and deletion mapping of *Escherichia coli* mutants defective in chemotaxis. *J. Bacteriol.* 135(1):45–53.